

Turbulent stagnation in a Z-pinch plasmaE. Kroupp, E. Stambulchik,^{*} A. Starobinets, D. Osin,[†] V. I. Fisher, D. Alumot,[‡] and Y. Maron
*Faculty of Physics, Weizmann Institute of Science, Rehovot 7610001, Israel*S. Davidovits[§] and N. J. Fisch
*Department of Astrophysical Sciences, Princeton University, Princeton, New Jersey 08540, USA*A. Fruchtman
H.I.T.—Holon Institute of Technology, Holon 5810201, Israel

(Received 16 May 2017; published 16 January 2018)

The ion kinetic energy in a stagnating plasma was previously determined by Kroupp *et al.* [*Phys. Rev. Lett.* **107**, 105001 (2011)] from Doppler-dominated line shapes augmented by measurements of plasma properties and assuming a uniform-plasma model. Notably, the energy was found to be dominantly stored in hydrodynamic flow. Here we advance a new description of this stagnation as supersonically turbulent. Such turbulence implies a nonuniform density distribution. We demonstrate how to reanalyze the spectroscopic data consistent with the turbulent picture and show that this leads to better concordance of the overconstrained spectroscopic measurements, while also substantially lowering the inferred mean density.

DOI: [10.1103/PhysRevE.97.013202](https://doi.org/10.1103/PhysRevE.97.013202)**I. INTRODUCTION**

In implosions of a cylindrical Z-pinch plasma, hydrodynamic kinetic motion is ultimately transferred to thermal motion of plasma particles—electrons and ions—through a cascade of atomic and thermodynamic processes [1–4]. These processes culminate at the stagnation phase, producing high-energy-density plasmas and generating powerful x-ray and neutron radiation [5].

Previous x-ray spectroscopic analysis of pinch plasmas [6,7] found that the ion kinetic energy at the stagnation phase was dominantly nonthermal hydrodynamic motion, while the plasma appeared largely uniform at spatial and temporal scales down to at least $100\ \mu\text{m}$ and $\sim 1\ \text{ns}$, respectively. An explanation of this phenomenon has been offered [8], where simulations showed steep radial velocity gradients in the stagnation region. On the other hand, we note here that the Reynolds number in the stagnating plasma is initially high ($\sim 10^5$), making turbulence a candidate for such significant small-scale hydrodynamic motion [the two-dimensional (2D) simulations in Ref. [8] would not be expected to reproduce turbulent behavior]. The inferred Mach numbers, M , at stagnation are supersonic, see Table I for Re and M . Were supersonic turbulence present, it would imply substantial nonuniformity in quantities such as the density (see, e.g., Fig. 2 in Ref. [9]). However, the previous analysis [6] assumed a uniform plasma.

This study reanalyzes the experimental data [6] without assuming uniformity, using, instead, a modeled turbulent

density distribution [10]. In doing so, we give a new physical description of a stagnated plasma dominated by supersonic turbulence using a spectroscopic analysis method. We find full (actually, improved) consistency with the observations but a significantly (about two-fold) lower average density. The results are believed to also be relevant for large-scale Z-pinch devices, inertial confinement experiments with large residual hydrodynamic motion, and in various astrophysical contexts.

II. SHORT DESCRIPTION OF THE PREVIOUS STUDY

In brief, a 9-mm-long neon-puff Z-pinch was imploded in 500 ns under a current rising to 500 kA at the stagnation time. Experimental diagnostics included high-resolution ($\sim 200\ \mu\text{m}$) gated x-ray filtered-pinhole imaging, a spectrometer recording Ne He-like dielectronic satellites with a resolving power of 6700 and a photoconductive detector (PCD) sensitive to $\hbar\omega \gtrsim 700\ \text{eV}$ radiation. All the data were *simultaneously* acquired over the stagnation period, about $\pm 5\ \text{ns}$ around the peak of the PCD signal with a time resolution of $\sim 1\ \text{ns}$. A plasma segment at $z = 5 \pm 1\ \text{mm}$ along the pinch axis was used for the analysis.

The modeling assumed a uniform-cylinder plasma with a prescribed (within experimental uncertainties) time evolution of T_e , n_e , and plasma radius r_{pl} . The experimental data and uniform model parameters are shown in Table I. Assuming uniformity, the electron density n_e was determined based on the satellite-intensity ratio [11,12]; it is n_e^0 in the table. A separately measured time-integrated continuum slope [13] was found to agree with the $T_e(t)$ assumed. The x-ray images give r_{pl} to within the $\sim 200\text{-}\mu\text{m}$ resolution, $r_{\text{min}}, r_{\text{max}}$ in Table I. The self-consistency of the uniform-model time dependencies for n_e , T_e , and r_{pl} was verified using the additional measurement of the absolutely calibrated PCD signal, which is sensitive to all

^{*}Corresponding author: evgeny.stambulchik@weizmann.ac.il[†]Present address: Tri Alpha Energy Inc, Foothill Ranch, CA, USA.[‡]Present address: Applied Materials, Rehovot, Israel.[§]Corresponding author: sdavidov@princeton.edu

TABLE I. The experimental data [6] relevant for the analysis presented; the plasma parameters assumed for $(r_{\text{pl}}^0, n_e^0, T_e)$ and inferred from (T_i, M, Re) the *uniform-plasma* modeling; the calculated isothermal turbulence parameters, volumetric density factor β , and, respectively, corrected plasma electron density and radius. Units are as follows: all radii are in mm, all temperatures are in eV, and densities are in 10^{20} cm^{-3} .

Experimental data						Uniform plasma						Isothermal turbulence						
t (ns)	δR	I_{PCD} (GW)	r_{min}	r_{max}	T_i^{eff}	r_{pl}^0	n_e^0	T_e	T_i	M	Re	θ	$\sigma_{s,v}^2$	$\langle \xi_V^2 \rangle$	$\langle \xi_V^3 \rangle$	β	n_e^{turb}	$r_{\text{pl}}^{\text{turb}}$
-3.4	0.15	0.35 ± 0.3	0.19	0.41	3000	0.23	6.0	120	250	2.4	8.1×10^4	0.048	0.70	1.84	5.77	0.32	1.9	0.53
-2.0	0.15	2.0 ± 1.0	0.25	0.47	2100	0.29	6.0	175	230	1.7	6.9×10^4	0.034	0.40	1.44	2.86	0.54	3.2	0.45
-1.2	0.15	3.8 ± 1.1	0.36	0.52	1800	0.31	6.0	190	210	1.6	7.7×10^4	0.032	0.36	1.39	2.60	0.60	3.6	0.44
0.0	0.15	6.5 ± 0.7	0.46	0.68	1300	0.35	6.0	185	200	1.3	8.9×10^4	0.026	0.25	1.26	1.96	0.57	3.4	0.55
2.0	0.15	3.6 ± 1.0	0.36	0.53	900	0.24	6.0	155	180	1.2	7.4×10^4	0.024	0.21	1.22	1.80	0.53	3.2	0.41
3.3	0.15	2.3 ± 0.9	0.21	0.43	720	0.20	6.0	140	180	1.0	5.1×10^4	0.020	0.15	1.16	1.53	0.62	3.7	0.30

three quantities. With T_e fixed, it was found that *either* n_e or r_{pl} could be taken at the center of its measured value range (i.e., uncertainty), with the other quantity then within one or two standard deviations of its independently measured value. With n_e the more important quantity, it was chosen to let r_{pl} vary outside one deviation; this gave r_{pl}^0 in Table I.

III. NEW MODEL

Although the uniform plasma analysis was reasonably consistent with the data, the uniform density assumption will not be *physically sound* if the plasma is highly turbulent, as expected for the measured Re and M . Therefore, we use a (nonuniform) turbulent plasma model. Within such a model, all plasma properties—density ρ , electron T_e and ion T_i temperatures, and the nonthermal ion velocity v_{flow} —have certain distributions, with possible correlations between them. This work analyzes the simplest case, of isothermal turbulence, where T_e and T_i are uniform (see the discussion below), whereas ρ (and n_e) are not. Then the previous spectral fits and T_e analysis are still valid because the correlation between turbulent velocity and density is very weak for isothermal turbulence [9], and the turbulent velocity distribution is well approximated by a Gaussian (see, e.g., Refs. [14–16]), which was also the assumed nonthermal velocity distribution used in the original study [6]. This leaves T_i^{eff} inferred from Doppler broadening [12] unaffected. We now show that, using a turbulent density probability distribution function (PDF) that is consistent with the measured Re and M , the inferred density is substantially reduced, which allows the inferred plasma radius at each time to be larger, while staying consistent with the PCD signal. This larger radius now agrees well with $[r_{\text{min}}, r_{\text{max}}]$ (except at the first measurement time, which has the weakest signal). Thus, the new turbulent model is an improvement *both* because it is physically sound *and* gives an improved match to the observations.

We work with electron density n_e instead of mass density ρ , since the atomic experimental data are sensitive to n_e . The two are related, $\rho = \langle Z_i \rangle^{-1} m_i n_e$, where $\langle Z_i \rangle$ is the mean ion charge and m_i is the ion mass. In principle, $\langle Z_i \rangle$ is a function of T_e and n_e , but for the ranges of plasma parameters of interest, it varies very weakly [6,8], so we assume $\rho \propto n_e$.

For each measurement the density has a PDF, $P(n_e)$. The previous data analysis [6] corresponds to $P(n_e) \equiv \delta(n_e - n_e^0)$. $P(n_e)$'s are different at different times and z positions, i.e., $P(t, z; n_e)$; for brevity, these t, z labels will be omitted.

Let us switch to dimensionless quantity

$$\xi \equiv n_e/n_e^0; \int P(\xi) d\xi = 1. \quad (1)$$

The average density is $\langle n_e \rangle = n_e^0 \int \xi P(\xi) d\xi$. It is important to note that $\langle n_e \rangle$ is not the same as n_e^0 . The nonuniform density affects two of the previous measurements: n_e from line ratios and the absolutely calibrated PCD signal, from which one can infer the radiating mass (product of n_e and r_{pl}^2), for a given T_e . These measurements give two constraints on the turbulent PDF, $P(\xi)$, which thus determine the new mean density.

Assuming the collisional-radiative equilibrium is established much faster than the hydromotion, the intensity of a discrete spectral line or continuum radiation in a turbulent plasma can be obtained in the static approximation [17], viz.,

$$\langle I \rangle = \int \epsilon(\vec{r}) d^3 r = \pi r_{\text{pl}}^2 \ell \int \epsilon(\xi) P(\xi) d\xi. \quad (2)$$

Here ϵ is the local plasma emissivity, approximately scaling as $\propto \xi^2$ if the density does not vary too much, ℓ is the length (in the z direction) of the plasma segment being analyzed, and we assumed that density variations are independent of r . In particular, the PCD signal is

$$I_{\text{PCD}} \propto \pi r_{\text{pl}}^2 \ell \int \xi^2 P(\xi) d\xi. \quad (3)$$

Using this, and the fact that the previous model described I_{PCD} self-consistently (within the errors bars δI_{PCD}) by assuming r_{pl}^0 , we can get a first constraint on $P(\xi)$, bounding I_{PCD} with r_{min} and r_{max} and $\pm \delta I_{\text{PCD}}$,

$$\left(1 - \frac{\delta I_{\text{PCD}}}{I_{\text{PCD}}}\right) \left(\frac{r_{\text{pl}}^0}{r_{\text{max}}}\right)^2 \leq \int \xi^2 P(\xi) d\xi \leq \left(1 + \frac{\delta I_{\text{PCD}}}{I_{\text{PCD}}}\right) \left(\frac{r_{\text{pl}}^0}{r_{\text{min}}}\right)^2. \quad (4)$$

Some of the autoionizing dielectronic satellites have even stronger density dependence than $\propto \xi^2$ —which is why the intensity ratio of such a satellite to another line (in our case—another close-by dielectronic satellite) allows for inferring the density [11]. Both dependencies are complex, but around the density point of interest ($\sim 5 \times 10^{20} \text{ cm}^{-3}$), their ratio is rather close to a linear form, $R \approx R^0 + a_R(n_e/n_e^0 - 1)$, in a steady-state optically thin plasma (see Fig. 1). Hence, if n_e does

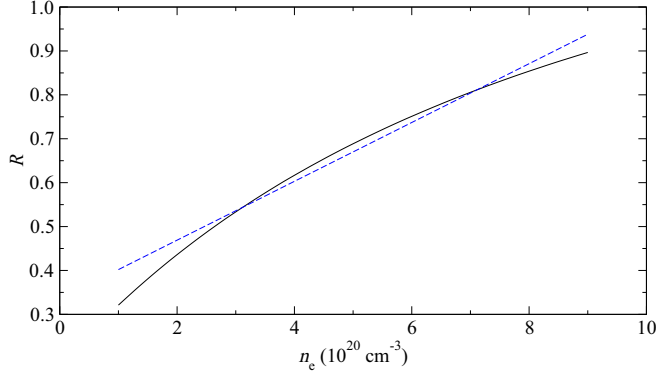


FIG. 1. $2p^2(^3P) \rightarrow 1s2p(^3P) \rightarrow 2s2p(^3P) \rightarrow 1s2s(^3S)$ intensity ratio (the solid line) and its linear approximation (the dashed line) calculated [18] as a function of n_e . Optically thin steady-state plasma with $T_e = 200$ eV is assumed.

not vary too wildly, (say, within a factor $\times 2$ in each direction), then

$$\langle R \rangle = R^0 + a_R \frac{\int (\xi - 1) \xi^2 P(\xi) d\xi}{\int \xi^2 P(\xi) d\xi}. \quad (5)$$

The measured quantity R_{expt} is known within its error bars, i.e., $\langle R \rangle = R_{\text{expt}} = R^0 \pm \delta R$. Therefore, Eq. (5) gives a second constraint on $P(\xi)$,

$$1 - \frac{\delta R}{a_R} \leq \frac{\int \xi^3 P(\xi) d\xi}{\int \xi^2 P(\xi) d\xi} \leq 1 + \frac{\delta R}{a_R}. \quad (6)$$

To model the density PDF that would result from turbulence in the stagnating plasma, we use the PDF of Hopkins [10]. Since the model assumes the average density is known, it is convenient to introduce dimensionless *volumetric* density by normalizing to $\langle n_e \rangle$, i.e., $\xi_V \equiv n_e / \langle n_e \rangle$. Evidently, $\xi / \xi_V = \langle n_e \rangle / n_e^0$. In terms of ξ_V , the (volumetric) PDF is

$$P_V(\xi_V) d\xi_V = \frac{I_1[2\sqrt{\lambda\omega(\xi_V)}]}{\exp[\lambda + \omega(\xi_V)]} \sqrt{\frac{\lambda}{\theta^2\omega(\xi_V)}} \frac{d\xi_V}{\xi_V}, \quad (7)$$

where $\lambda \equiv \sigma_{s,V}^2 / 2\theta^2$, $\omega(\xi_V) \equiv \lambda / (1 + \theta) - \ln(\xi_V) / \theta$, and I_1 is the modified Bessel function of the first kind. This two-parameter PDF depends on a variance, $\sigma_{s,V}^2$, and a measure of intermittency, θ . As $\theta \rightarrow 0$, the PDF becomes log-normal. This PDF fits well for simulations conducted at a wide range of Mach numbers [10]. Although we presently treat the turbulence as isothermal, this PDF has been shown to fit for simulations of nonisothermal turbulence [19]. In general, the values of, $\sigma_{s,V}^2, \theta$, depend on the turbulence properties; they are typically modeled as depending on the turbulent Mach number, the mix of compressive and solenoidal forcing, and, in the nonisothermal case, the polytropic gamma [10,19]. As such, the turbulence model does not introduce any “free” parameters, since its parameters vary only as a direct consequence of the variation of measured or inferred plasma properties.

For the value of θ , we use the fit to simulation data [10], which is $\theta \approx 0.05M_c$. Here M_c is the compressive Mach number, also written $M_c = bM$ [20,21], and b is related to the mix of solenoidal and compressive modes [20–22]. For the density variance, $\sigma_{s,V}^2$, we combine the usual isother-

mal logarithmic density variance (see, e.g., Refs. [23–26]), $\sigma_s^2 \approx \ln[1 + b^2M^2]$, with the relationships $\sigma_{s,V}^2 = (1 + \theta)^3 \sigma_{s,M}^2$ [10] and $\sigma_s^2 = \sigma_{s,V} \sigma_{s,M}$ [19]. This yields $\sigma_{s,V}^2 = (1 + \theta)^{3/2} \ln[1 + b^2M^2]$. Here we take $b = 0.4$; see the discussion below for more on this choice and caveats associated with the turbulence model.

The Mach number at each time is calculated using the data in Table I; $M = v_{\text{flow}} / c_s$, where $v_{\text{flow}} = [3(T_i^{\text{eff}} - T_i) / m_i]^{1/2}$ and $c_s = [\gamma(T_e n_e + T_i n_i) / (n_i m_i + n_e m_e)]^{1/2}$, where $\gamma = 1$ is used, assuming isothermality (discussed below).

IV. RESULTS AND DISCUSSION

We now use the turbulent density PDF, Eq. (7), in the constraints (4) and (6). In addition to satisfying the usual normalization condition, Eq. (1), it also conserves the average density, $\int \xi_V P_V(\xi_V) d\xi_V = 1$. However, experimentally the average density is unknown; in order to use the volumetric PDF and its moments, we connect ξ and ξ_V with a free parameter β , $\xi = \beta \xi_V$. Once the turbulence PDF satisfying the experimental data within the constraints (4) and (6) is determined, βn_e^0 will give the new mean density, corrected for the presence of turbulence; more generally, $\langle \xi^k \rangle = \beta^k \langle \xi_V^k \rangle$. With this in mind, Eqs. (4) and (6) become a set of inequalities on β ,

$$\sqrt{\frac{1 - \frac{\delta I_{\text{PCD}}}{I_{\text{PCD}}} r_{\text{pl}}^0}{\langle \xi_V^2 \rangle} \frac{r_{\text{pl}}^0}{r_{\text{max}}}} \leq \beta \leq \sqrt{\frac{1 + \frac{\delta I_{\text{PCD}}}{I_{\text{PCD}}} r_{\text{pl}}^0}{\langle \xi_V^2 \rangle} \frac{r_{\text{pl}}^0}{r_{\text{min}}}}, \quad (8)$$

$$\left(1 - \frac{\delta R}{a_R}\right) \frac{\langle \xi_V^2 \rangle}{\langle \xi_V^3 \rangle} \leq \beta \leq \left(1 + \frac{\delta R}{a_R}\right) \frac{\langle \xi_V^2 \rangle}{\langle \xi_V^3 \rangle}, \quad (9)$$

shown graphically in Fig. 2(a). The new model predicts a significantly (about twofold) lower average density. With β chosen, the plasma radius needs to be corrected, accounting for the turbulence-modified average emissivity. Using Eq. (3), it follows that $r_{\text{pl}}^{\text{turb}} = r_{\text{pl}}^0 / \sqrt{\langle \xi^2 \rangle} = r_{\text{pl}}^0 / (\beta \sqrt{\langle \xi_V^2 \rangle})$. Notably, r_{pl} 's in the present model (listed as $r_{\text{pl}}^{\text{turb}}$ in Table I) fit the measured values better than the original model [6], as shown in Fig. 2(b).

For clarity, we have presented results in Fig. 2 with only experimental uncertainty. There are also uncertainties associated with the turbulence model. Changes in the results due to most of these uncertainties are primarily expected to be quantitative, with the picture of reduced mean density remaining. One uncertainty comes from the possibly nonequilibrium nature of any turbulence at stagnation. The turbulent velocity decreases in time during stagnation, as evidenced by the decreasing non-thermal energy excess per-ion ($T_i^{\text{eff}} - T_i$) in Table I. However, contrary to the turbulence simulations usually considered for modeling (e.g., in Ref. [10]), the total mass is not constant in time: At least initially, plasma continues to flow into the stagnation region. Using the isothermal turbulence r_{pl} and n_e in Table I, $r_{\text{pl}}^{\text{turb}}, n_e^{\text{turb}}$, along with a turbulent energy per particle of $T_i^{\text{eff}} - T_i$, yields a total turbulent energy in the stagnation region that remains relatively constant from $t = -3.4$ ns to $t = 0$ ns and then falls. Notably, the time scale for this observed fall (a few ns) is the dynamical time scale expected for supersonic turbulence [27,28] with these flow speeds and length scales; importantly, it is much faster than the viscous

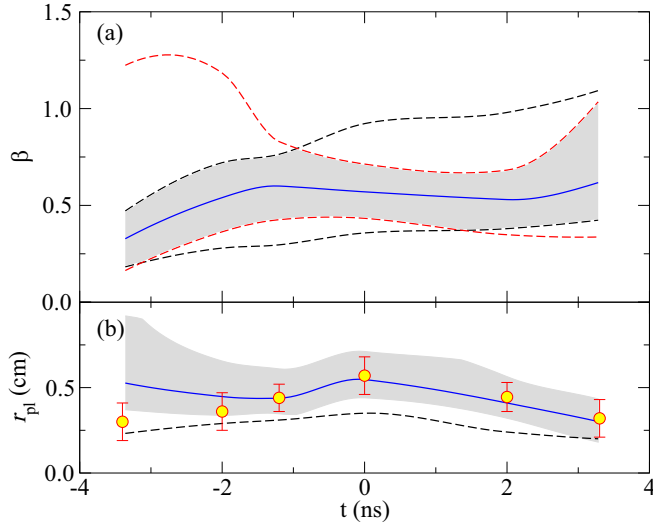


FIG. 2. (a) Limits of the double inequalities (8) and (9) are shown as red (gray) and black dashed lines, respectively. The ranges of β (corrected density $n_e^{\text{trb}} = \beta n_e^0$) satisfying both inequalities are designated by the gray filled area, with the tentative values used to correct the uniform-model parameters indicated by the solid line. (b) r_{pl}^{trb} (the solid line, with the gray area denoting uncertainties) shows an improved agreement with the experimental data (symbols with error bars). r_{pl}^0 of the uniform-plasma model is given by the dashed line.

time scale, without a cascade. Although the present density PDF model works in a variety of cases, it has typically been tested in situations with equilibrium forcing, which may not be the best analog for the present case.

Assuming the model applies, there are still uncertainties. One is the degree to which turbulence in this stagnating plasma would be isothermal. Conduction and turbulent time scales are not well separated, so that an accurate determination of the degree of isothermality would likely require detailed simulations, as in other topic areas [29,30]. The turbulence model used here applies in the nonisothermal case, with different θ , $\sigma_{s,v}^2$ [19]. At this level, nonisothermality is expected to only modestly change the parameters in Table I, although then the inferred T_e and M will also need to be reconsidered, because nonisothermality would have a pronounced effect on the local plasma emissivity (it depends rather strongly on T_e), requiring modifications to Eqs. (2) and (5)—and therefore also to (8) and (9).

Any magnetic fields in the stagnating region could alter the values of θ and $\sigma_{s,v}^2$ [10,25,26], although the form of the PDF remains valid. These corrections should be small because the plasma pressure is much higher than the magnetic pressure in the stagnation region ($\beta_{\text{magnetic}} \gtrsim 20$) [31].

Even within the isothermal turbulence PDF model, there are uncertainties. Simulations show substantial spread in values of the PDF parameters around the expressions for θ and $\sigma_{s,v}^2$, see, e.g., Ref. [10]. Apart from modeling errors, spread in these values can be physical, due to the fluctuations of turbulence [32]. The correct value of b , presently taken to be $b = 0.4$, is uncertain. Generally, $b \in [1/3, 1]$ [9,22], with $b = 1/3$ occurring for solenoidal (divergence free) forcing [22]

and $b = 1$ occurring for compressive (curl-free) forcing. Equal parts solenoidal and compressive forcing gives $b \approx 0.4$ [9]. For a Z-pinch, one might expect largely compressive forcing. Given this uncertainty, one could calculate the range of β in Fig. 2(a) including also uncertainty in b . A larger b yields a lower range for β , while a smaller b yields a higher range.

The ion temperatures in Table I are inferred through a calculation involving the electron-ion temperature equilibration time [6]. Since this time is density dependent, it will be affected by density fluctuations. The equilibration time scale is faster in the high-density regions, which dominate the measurements; thus, the ion temperature may be driven slightly closer to the electron temperature. Since the electron-ion temperature equilibration time scale is already very fast, this is expected to cause T_i to be a few percent lower than in Ref. [6].

The underlying atomic model used for the present analysis is the same as in the previous study [6] and, therefore, no additional uncertainties have been introduced. In fact, the associated inaccuracy may be surprisingly low, as the Monte Carlo analysis of uncertainty propagation in collisional-radiative models indicates [33]. So far, we have neglected possible opacity effects. Fortunately, the satellites used have a negligible optical thickness. The bound-free and free-free (bremsstrahlung) radiation that contributes to the PCD signal is also optically thin; however, strong bound-bound transitions are not. This requires a modification of Eq. (2) which cannot be represented analytically. However, the plasma absorption coefficients, similar to the emission ones, for these transitions scale as n_e^2 . Therefore, the difference from the uniform-plasma model (in which the opacity was properly accounted for numerically) should vanish in the lowest order.

The mechanism generating the (nonradial) hydrodynamic motion is unclear; while energy is dumped in the hydrodynamic motion in the process of stagnation [7], this hydrodynamic motion could be seeded by turbulence generated and carried along during the compression itself or could be generated entirely at stagnation. In either event, there are important implications for Z-pinchs and more broadly.

If the (turbulent) hydromotion is generated and carried along during the compression, then these Z-pinchs represent a test bed for the properties of plasma turbulence undergoing compression. These properties are relevant for a proposed novel fast ignition or x-ray burst generation scheme [34,35]. Of particular interest is that the present hydromotion is supersonic, the regime in which these schemes would operate. Further, the behavior of compressing supersonic turbulence is of critical interest in astrophysics, particularly for molecular cloud dynamics [36,37]. Supersonic turbulence behavior has been related to the star formation efficiency [38], the core mass or stellar initial mass functions [39–41], and Larson's laws [42].

If the hydrodynamic motion is generated at stagnation, and then decays, then its properties could still be of astrophysical interest (see, e.g., Refs. [14,16,27–30,32,37,43]). To the extent generation and/or decay of the hydrodynamic motion at stagnation can be observed, studies of supersonic turbulence in Z-pinchs could serve as a new and important area for laboratory astrophysics. Indeed, in the present study, not all values of the turbulent PDF parameters, $\theta, \sigma_{s,v}^2$, will be consistent with the observations; more measurements could help to constrain turbulent properties. Z-pinchs such as the present

may yield other cross-over opportunities with astrophysics, for example, in turbulent density PDF measurement techniques (e.g., Refs. [43,44]) or in mechanisms for turbulent generation and forcing in complex plasma environments (e.g., Ref. [45]).

The present analysis is likely relevant to high-current implosions, like Z-pinch experiments on the Z machine [46]. Indeed, based on the plasma parameters given in Ref. [7], Re is also high ($\sim 10^4$), and M is similar to the case analyzed here. This analysis may also be relevant in inertial confinement experiments that observe large quantities of residual hydrodynamic motion.

Even though the present experiments are very well diagnosed by Z-pinch standards, one should consider additional measurements for verifying the picture of a turbulent stagnation. To this end, other spectroscopy methods can be useful. For example, one can try to study the density by the use of the Stark broadening of high- n transitions in hydrogen-like Ne or lower- Z species (C, N, or O) that can be mixed with the puffed neon.

In summary, a new analysis of stagnating pinch data, replacing the assumption of uniform plasma with density variations consistent with a turbulent plasma, advances a picture of

superpersonally turbulent stagnating plasma. This picture is not only consistent with the observations but also improves the agreement with them. The mean plasma density is reduced by a factor ~ 2 . While there is uncertainty in the precise value of this reduction, the general picture, of a data analysis in the presence of highly turbulent stagnating plasma reducing the inferred stagnation density compared to the uniform case, is believed to be robust and widely relevant. Beyond aiding our understanding of Z-pinchs, we hope this study has shown fertile ground for relation to problems of astrophysical interest.

ACKNOWLEDGMENTS

Y.M. is grateful to M. Herrmann, A. L. Velikovich, and E. P. Yu for enlightening discussions. This work was supported by BSF-NSF (USA) and BSF 2014714. The work of E.K., E.S., A.S., V.I.F., and Y.M. was supported in part by the Israel Science Foundation and the DOE-Cornell University Excellence Center (USA). The work of S.D. and N.J.F. was supported by NNSA 67350-9960 (Prime Grant No. DOE DE-NA0001836) and by NSF Contract No. PHY-1506122.

-
- [1] D. D. Ryutov, M. S. Derzon, and M. K. Matzen, *Rev. Mod. Phys.* **72**, 167 (2000).
 - [2] S. A. Slutz and R. A. Vesey, *Phys. Rev. Lett.* **108**, 025003 (2012).
 - [3] M. Herrmann, *Nature* **506**, 302 (2014).
 - [4] D. B. Sinars, E. M. Campbell, M. E. Cuneo, C. A. Jennings, K. J. Peterson, and A. B. Sefkow, *J. Fusion Energ.* **35**, 78 (2016).
 - [5] J. L. Giuliani and A. S. Safronova, *Phys. Plasmas* **23**, 101101 (2016).
 - [6] E. Kroupp, D. Osin, A. Starobinets, V. Fisher, V. Bernshtam, L. Weingarten, Y. Maron, I. Uschmann, E. Förster, A. Fisher, M. E. Cuneo, C. Deeney, and J. L. Giuliani, *Phys. Rev. Lett.* **107**, 105001 (2011).
 - [7] Y. Maron, A. Starobinets, V. I. Fisher, E. Kroupp, D. Osin, A. Fisher, C. Deeney, C. A. Coverdale, P. D. Lepell, E. P. Yu, C. Jennings, M. E. Cuneo, M. C. Herrmann, J. L. Porter, T. A. Mehlhorn, and J. P. Apruzese, *Phys. Rev. Lett.* **111**, 035001 (2013).
 - [8] J. L. Giuliani, J. W. Thornhill, E. Kroupp, D. Osin, Y. Maron, A. Dasgupta, J. P. Apruzese, A. L. Velikovich, Y. K. Chong, A. Starobinets, V. Fisher, Yu. Zarnitsky, V. Bernshtam, A. Fisher, T. A. Mehlhorn, and C. Deeney, *Phys. Plasmas* **21**, 031209 (2014).
 - [9] C. Federrath, J. Roman-Duval, R. S. Klessen, W. Schmidt, and M.-M. Mac Low, *Astron. Astrophys.* **512**, A81 (2010).
 - [10] P. F. Hopkins, *Mon. Not. R. Astron. Soc.* **430**, 1880 (2013).
 - [11] J. F. Seely, *Phys. Rev. Lett.* **42**, 1606 (1979).
 - [12] E. Kroupp, D. Osin, A. Starobinets, V. Fisher, V. Bernshtam, Y. Maron, I. Uschmann, E. Förster, A. Fisher, and C. Deeney, *Phys. Rev. Lett.* **98**, 115001 (2007).
 - [13] D. Alumot, *Determination of the Temperature and Density of Hot-Dense Plasma by Measuring the x-Ray Continuum Spectra*, Master's thesis, Weizmann Institute of Science, Rehovot, Israel (2007).
 - [14] M. D. Smith, M.-M. Mac Low, and J. M. Zuev, *Astron. Astrophys.* **356**, 287 (2000).
 - [15] D. Porter, A. Pouquet, and P. Woodward, *Phys. Rev. E* **66**, 026301 (2002).
 - [16] S. Kitsionas, C. Federrath, R. Klessen, W. Schmidt, D. Price, L. Dursi, M. Gritschneider, S. Walch, R. Piontek, J. Kim *et al.*, *Astron. Astrophys.* **508**, 541 (2009).
 - [17] R. Stamm, I. Hannachi, M. Meireni, H. Capes, L. Godbert-Mouret, M. Koubiti, J. Rosato, Y. Marandet, M. Dimitrijević, and Z. Simić, *Eur. Phys. J. D* **71**, 68 (2017).
 - [18] Yu. V. Ralchenko and Y. Maron, *J. Quant. Spectr. Rad. Transfer* **71**, 609 (2001).
 - [19] C. Federrath and S. Banerjee, *Mon. Not. R. Astron. Soc.* **448**, 3297 (2015).
 - [20] L. Konstandin, P. Girichidis, C. Federrath, and R. S. Klessen, *Astrophys. J.* **761**, 149 (2012).
 - [21] L. Konstandin, W. Schmidt, P. Girichidis, T. Peters, R. Shetty, and R. S. Klessen, *Mon. Not. R. Astron. Soc.* **460**, 4483 (2016).
 - [22] C. Federrath, R. S. Klessen, and W. Schmidt, *Astrophys. J. Lett.* **688**, L79 (2008).
 - [23] P. Padoan, Å. Nordlund, and B. J. T. Jones, *Mon. Not. R. Astron. Soc.* **288**, 145 (1997).
 - [24] T. Passot and E. Vázquez-Semadeni, *Phys. Rev. E* **58**, 4501 (1998).
 - [25] P. Padoan and Å. Nordlund, *Astrophys. J.* **730**, 40 (2011).
 - [26] F. Z. Molina, S. C. O. Glover, C. Federrath, and R. S. Klessen, *Mon. Not. R. Astron. Soc.* **423**, 2680 (2012).
 - [27] M.-M. Mac Low, R. S. Klessen, A. Burkert, and M. D. Smith, *Phys. Rev. Lett.* **80**, 2754 (1998).
 - [28] M.-M. Mac Low, *Astrophys. J.* **524**, 169 (1999).
 - [29] G. Pavlovski, M. D. Smith, M.-M. Mac Low, and A. Rosen, *Mon. Not. R. Astron. Soc.* **337**, 477 (2002).
 - [30] G. Pavlovski, M. D. Smith, and M.-M. Mac Low, *Mon. Not. R. Astron. Soc.* **368**, 943 (2006).
 - [31] G. Rosenzweig, E. Kroupp, A. Starobinets, A. Fisher, and Y. Maron, in *2014 IEEE 41st International Conference on Plasma Sciences (ICOPS 2014)* (Institute of Electrical and Electron-

- ics Engineers (IEEE), Washington, DC, USA, 2015), Vol. 1, p. 35.
- [32] M. N. Lemaster and J. M. Stone, *Astrophys. J. Lett.* **682**, L97 (2008).
- [33] Yu. Ralchenko, in *Modern Methods in Collisional-Radiative Modeling of Plasmas*, edited by Yu. Ralchenko, Springer Series on Atomic, Optical, and Plasma Physics No. 90 (Springer, Berlin, 2016), pp. 181–208.
- [34] S. Davidovits and N. J. Fisch, *Phys. Rev. Lett.* **116**, 105004 (2016).
- [35] S. Davidovits and N. J. Fisch, *Phys. Rev. E* **94**, 053206 (2016).
- [36] B. Robertson and P. Goldreich, *Astrophys. J. Lett.* **750**, L31 (2012).
- [37] S. Davidovits and N. J. Fisch, *Astrophys. J.* **838**, 118 (2017).
- [38] B. G. Elmegreen, *Astrophys. J.* **672**, 1006 (2008).
- [39] P. Padoan and A. Nordlund, *Astrophys. J.* **576**, 870 (2002).
- [40] J. Ballesteros-Paredes, A. Gazol, J. Kim, R. S. Klessen, A.-K. Jappsen, and E. Tejero, *Astrophys. J.* **637**, 384 (2006).
- [41] P. Hennebelle and G. Chabrier, *Astrophys. J.* **684**, 395 (2008).
- [42] A. G. Kritsuk, C. T. Lee, and M. L. Norman, *Mon. Not. R. Astron. Soc.* **436**, 3247 (2013).
- [43] E. C. Ostriker, J. M. Stone, and C. F. Gammie, *Astrophys. J.* **546**, 980 (2001).
- [44] C. M. Brunt, C. Federrath, and D. J. Price, *Mon. Not. R. Astron. Soc.* **403**, 1507 (2010).
- [45] M. Gritschneder, T. Naab, S. Walch, A. Burkert, and F. Heitsch, *Astrophys. J. Lett.* **694**, L26 (2009).
- [46] B. Jones, C. Deeney, C. Coverdale, P. LePell, J. McKenney, J. Apruzese, J. Thornhill, K. Whitney, R. Clark, A. Velikovich, J. Davis, Y. Maron, V. Kantsyrev, A. Safronova, and V. Oreshkin, *J. Quant. Spectr. Rad. Transfer* **99**, 341 (2006).